
Topological Autoencoders

Michael Moor^{*†}

michael.moor@bsse.ethz.ch

Max Horn^{*†}

max.horn@bsse.ethz.ch

Bastian Rieck^{*‡}

bastian.rieck@bsse.ethz.ch

Karsten Borgwardt^{*‡}

karsten.borgwardt@bsse.ethz.ch

Abstract

We propose a novel approach for preserving topological structures of the input space in latent representations of autoencoders. Using *persistent homology*, a technique from topological data analysis, we calculate topological signatures of both the input and latent space to derive a topological loss term. Under weak theoretical assumptions, we can construct this loss in a differentiable manner, such that the encoding learns to retain multi-scale connectivity information. We show that our approach is theoretically well-founded, while exhibiting favourable latent representations on synthetic manifold data sets. Moreover, on real-world data sets, introducing our topological loss leads to more meaningful latent representations while preserving low reconstruction errors.

1 Introduction

While recently topological features, in particular the multi-scale features derived from persistent homology, have found increasing usage in the machine learning community [8, 25, 27, 43, 46], using topology *directly* as a constraint for current deep learning methods remains an unsolved problem. This is due to the inherently discrete nature of these computations, making backpropagation through the computation of topological signatures immensely difficult or only possible in certain special circumstances, such as assuming a fixed connectivity [41] or discretising a space [16].

In this work, we present a novel approach that permits us to obtain gradients during the computation of topological signatures. This permits employing topological constraints during training of deep neural networks and to build topology-preserving autoencoders based on the following contributions:

1. We develop a novel topological loss term for autoencoders that helps harmonise the topology of the data space and the topology of the latent space
2. We prove that our approach is stable on the level of mini-batches, resulting in suitable approximations of the persistent homology of a data set.
3. We empirically demonstrate that our novel loss term aids in dimensionality reduction by preserving topological structures in data sets; in particular, the learned latent representations are useful in that the preservation of topological structures can also aid interpretability.

^{*}Department of Biosystems Science and Engineering, ETH Zurich, 4058 Basel, Switzerland

[†]These authors contributed equally. Author order has been determined by tossing a virtual coin.

[‡]These authors jointly directed this work.

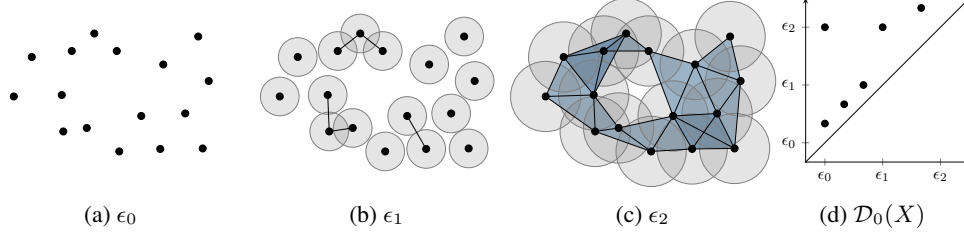


Figure 1: The Vietoris–Rips complex $\mathfrak{R}_\epsilon(X)$ of a point cloud X at different scales. As the distance threshold ϵ is increased, the connectivity changes. The creation and destruction of d -dimensional topological features is recorded in the d^{th} persistence diagram $\mathcal{D}_0(X)$.

2 Background: Persistent homology

Persistent homology [20, 21] is a method from the emerging field of computational topology, which develops tools for analysing topological features of data sets. Such features describe the *connectivity* of data, for example in the form of connected components. To give an intuitive description of persistent homology, we first need to introduce the concept of simplicial homology. For a simplicial complex \mathfrak{K} , i.e. a generalised graph with higher-order connectivity information, simplicial homology employs reduction algorithms on a boundary matrix to assign \mathfrak{K} a family of groups, the *homology groups*. The d^{th} homology group $H_d(\mathfrak{K})$ of \mathfrak{K} contains d -dimensional topological features, such as connected components ($d = 0$), cycles/tunnels ($d = 1$), and voids ($d = 2$). Elements of $H_d(\mathfrak{K})$ are typically summarised as counts, making them a simple invariant “signature” of a manifold. For example, a circle in \mathbb{R}^2 has one feature with $d = 1$ (a cycle), and one feature with $d = 0$ (a connected component).

When working with real-world data, the underlying manifold \mathbb{M} is usually unknown. Instead, we are working with a point cloud $X := \{x_1, \dots, x_n\} \subseteq \mathbb{R}^d$ and a metric $\text{dist}: X \times X \rightarrow \mathbb{R}$ such as the Euclidean distance. Persistent homology now extends simplicial homology to this setting; instead of approximating \mathbb{M} by means of a *single* simplicial complex, which would be a brittle and error-prone procedure due to the discrete nature of X , persistent homology analyses changes in the homology groups over *multiple* scales of the metric. This is achieved by constructing a special simplicial complex, the Vietoris–Rips complex [53, 56]. For $0 \leq \epsilon < \infty$, the Vietoris–Rips complex of X at scale ϵ , denoted by $\mathfrak{R}_\epsilon(X)$, contains all simplices (i.e. subsets) of X for which $\text{dist}(x_i, x_j) \leq \epsilon$ holds for all i, j . Given a matrix \mathbf{A} of pairwise distances of a point cloud X , we will use $\mathfrak{R}_\epsilon(\mathbf{A})$ and $\mathfrak{R}_\epsilon(X)$ interchangeably. Vietoris–Rips complexes of different thresholds satisfy a nesting relation, i.e. $\mathfrak{R}_{\epsilon_i}(X) \subseteq \mathfrak{R}_{\epsilon_j}(X)$ for $\epsilon_i \leq \epsilon_j$, so it is possible to track changes in the homology groups as ϵ increases; see the seminal algorithm Edelsbrunner et al. [22] for more details. Figure 1 illustrates this process. Moreover, since X contains a finite number of points, a maximum ϵ value exists after which the connectivity does not change any more; it is thus sufficient to calculate \mathfrak{R}_ϵ to obtain information about topological features at all scales.

We write $\text{PH}(\mathfrak{R}_\epsilon(X))$ for the persistent homology calculation of the Vietoris–Rips complex. It results in a tuple $(\{\mathcal{D}_1, \mathcal{D}_2, \dots\}, \{\pi_1, \pi_2, \dots\})$ of *persistence diagrams* (first component) and *persistence pairings* (second component). The d -dimensional persistence diagram \mathcal{D}_d of $\mathfrak{R}_\epsilon(X)$ contains coordinates of the form (a, b) , where a refers to a threshold ϵ at which a d -dimensional topological feature is created in Vietoris–Rips complex, and b refers to a threshold ϵ' at which it is destroyed. See Figure 1d for an illustration. If $d = 0$, for example, the threshold ϵ' indicates at which distance two connected components in X are merged into one; this is related to spanning trees [31]. The d -dimensional persistence pairing contains indices (i, j) corresponding to simplices $s_i, s_j \in \mathfrak{R}_\epsilon(X)$ that create and destroy the topological feature identified by $(a, b) \in \mathcal{D}_d$, respectively. Persistence diagrams are known to be stable with respect to small perturbations in the data set [11, 15, 18]. Two persistence diagrams \mathcal{D} and \mathcal{D}' can be compared using the *bottleneck distance*

$$d_b(\mathcal{D}, \mathcal{D}') := \inf_{\eta: \mathcal{D} \rightarrow \mathcal{D}'} \sup_{x \in \mathcal{D}} \|x - \eta(x)\|_\infty, \quad (1)$$

where $\eta: \mathcal{D} \rightarrow \mathcal{D}'$ denotes a bijection between the points of the two diagrams, and $\|\cdot\|_\infty$ refers to the L_∞ norm. This calculation is extended to multiple diagrams of varying dimensions by summing over the corresponding distances according to Eq. 1. We denote the space of persistence diagrams as

\mathfrak{D} and to simplify notation, we use $\mathcal{D}(X) \subseteq \mathfrak{D}$ to refer to the set of persistence diagrams of a point cloud X arising from $\text{PH}(\mathfrak{R}_\epsilon(X))$.

3 Proposed method: Topology-preserving autoencoders

We propose a generic framework for constraining autoencoders to preserve topological structures (measured via persistent homology) of the data space in their latent encodings. In Section 3.1, we outline the calculation of a Vietoris–Rips complex for obtaining the persistent homology of a point cloud. We then apply the results of this calculation in Section 3.2 to build an autoencoder with a novel *topological loss* term. In Section 3.3, we show that this loss term is differentiable under weak theoretical assumptions and can thus be directly used in backpropagation. Finally, Section 3.4 discusses theoretical properties concerning the stability of our method.

3.1 Vietoris–Rips complex calculation

Given a finite metric space \mathcal{S} , such as a subsample of the original data, we first calculate the persistent homology of the Vietoris–Rips filtration of its distance matrix $\mathbf{A}^\mathcal{S}$. To this end, let $\epsilon := \max \mathbf{A}^\mathcal{S}$ and $\mathfrak{R}_\epsilon(\mathbf{A}^\mathcal{S})$ be the corresponding Vietoris–Rips complex as described in Section 2. Given a maximum dimension⁴ of $d \in \mathbb{N}_{>0}$, we denote the resulting set of persistence diagrams as $\mathcal{D}(\mathcal{S}, d) \subseteq \mathfrak{D}$, and the set of persistence pairings as $\pi(\mathcal{S}, d)$.

Simplifying $\pi(\mathcal{S}, d)$ The d -dimensional persistence pairing π_d contains indices of simplices that are relevant for creating and destroying d -dimensional topological features. We observe that we can consider each pairing to represent *edge indices*, namely the edges that are deemed to be “topologically relevant” by the computation of persistent homology (see below for more details). This works because the Vietoris–Rips complex is a *clique complex*, i.e. it is fully determined by its edges [56]. Since the Vietoris–Rips calculation only depends on the fixed distance matrix of a given space, we will also write $\pi^\mathcal{S}$ to refer to the persistence pairings that result from $\text{PH}(\mathfrak{R}_\epsilon(\mathbf{A}^\mathcal{S}))$.

Obtaining edge indices For 0-dimensional topological features, it is sufficient to look at the *edge indices*, i.e. the indices of “destroyer” simplices, contained in π_0 . Each of these indices corresponds to an edge in the minimum spanning tree of the data set. This calculation is computationally efficient, having a worst-case complexity of $\mathcal{O}(m^2 \cdot \alpha(m^2))$, where m is the batch size and $\alpha(\cdot)$ denotes the extremely slow-growing inverse of the Ackermann function [19, Chapter 22]. For 1-dimensional features, where edges are paired with triangles, we obtain edge indices by selecting the edge with the maximum weight of the triangle. While this procedure—and hence our method—generalises to higher dimensions, our implementation currently does not support higher-dimensional features.

3.2 Topological autoencoder

In the following, we consider a mini-batch X from the data space \mathcal{X} as a point cloud. Furthermore, we define an autoencoder as the composition of two functions $h \circ g$, where $g: \mathcal{X} \rightarrow \mathcal{Z}$ represents the *encoder* and $h: \mathcal{Z} \rightarrow \mathcal{X}$ represents the *decoder*. We denote latent codes with $Z := g(X^{(m)})$. During a forward pass of the autoencoder, we compute the persistent homology of the mini-batch in both the data as well as the latent space, yielding the following set of tuples:

$$(\mathcal{D}^X, \pi^X) := \text{PH}(\mathfrak{R}_\epsilon(X)) \quad \text{and} \quad (\mathcal{D}^Z, \pi^Z) := \text{PH}(\mathfrak{R}_\epsilon(Z)) \quad (2)$$

For better readability, we only consider the first set of components corresponding to the 0-dimensional persistence diagram returned by PH. In both cases, the values of the persistence diagram can be retrieved by subsetting the distance matrix with the indices provided by the persistence pairings, i.e. $\mathcal{D}^X \simeq \mathbf{A}^X[\pi^X]$. For notational purposes, we consider $\mathbf{A}^X[\pi^X]$ as a vector in $\mathbb{R}^{|\pi^X|}$. Informally speaking, the persistent homology calculation can thus be seen as a selection of topologically relevant edges of the Vietoris–Rips complex, followed by the selection of corresponding entries in the distance matrix. We compare both diagrams \mathcal{D}^X and \mathcal{D}^Z to construct a topological loss term \mathcal{L}_t , which we

⁴This means that we do not have to consider higher-dimensional topological features.

add to the standard reconstruction loss term \mathcal{L}_r to arrive at the following optimisation objective

$$\mathcal{L} = \mathcal{L}_r(X, h(g(X))) + \lambda \mathcal{L}_t, \quad (3)$$

where $\lambda \in \mathbb{R}$ is a parameter to control the strength of the regularisation.

3.3 Differentiable topological loss

We framed our calculation as a selection of relevant distances between a subset of samples. A straight-forward approach to impose the data space topology on the latent space would be to apply a loss on the selected distances in both spaces. However, such an approach cannot be stable as it merely compares topological features without matching the edges between $\mathfrak{R}_\epsilon(X)$ and $\mathfrak{R}_\epsilon(Z)$. A more elaborate approach would be to enforce similarity of the intersection of the selected edges in both complexes. When initialising a random latent space Z , the persistence pairing in the latent space could still select random edges, resulting in only 1 expected matched edge (independent of mini-batch size) between the two pairings. Thus, to obtain informative gradients and efficient training, we make use of both filtrations and account for the *union* of all selected edges in X and Z . To this end, our topological loss term decomposes into two components, each handling the “directed” loss occurring as topological features in one of the two spaces, i.e. either the data space X or the latent code Z , remain fixed. We have $\mathcal{L}_t = \mathcal{L}_{X \rightarrow Z} + \mathcal{L}_{Z \rightarrow X}$, where

$$\mathcal{L}_{X \rightarrow Z} := \frac{1}{2} \|\mathbf{A}^X[\pi^X] - \mathbf{A}^Z[\pi^X]\|^2 \quad \text{and} \quad \mathcal{L}_{Z \rightarrow X} := \frac{1}{2} \|\mathbf{A}^Z[\pi^Z] - \mathbf{A}^X[\pi^Z]\|^2, \quad (4)$$

respectively. The key idea for both terms is to align and preserve topologically relevant distances from both spaces. By taking the union of all selected edges (and the corresponding distances), we obtain an informative loss term that is determined by at least $|X|$ many distances. In case the topological structures of the two spaces X and Z are aligned perfectly, we have $\mathcal{L}_{X \rightarrow Z} = \mathcal{L}_{Z \rightarrow X} = 0$ because both pairings and their corresponding distances coincide.

We assume that there is an infinitesimal neighbourhood around each point in a persistence diagram that only contains this single point. Thus, the persistence pairing π does not change upon a small perturbation of the underlying distances. This guarantees the existences of the derivative of our topological loss. More precisely, our loss term permits calculating gradients for backpropagation. Letting θ refer to the parameters of the *encoder*, we have

$$\frac{\partial}{\partial \theta} \mathcal{L}_{X \rightarrow Z} = \frac{\partial}{\partial \theta} \left(\frac{1}{2} \|\mathbf{A}^X[\pi^X] - \mathbf{A}^Z[\pi^X]\|^2 \right) = -(\mathbf{A}^X[\pi^X] - \mathbf{A}^Z[\pi^X])^\top \left(\frac{\partial \mathbf{A}^Z[\pi^X]}{\partial \theta} \right) \quad (5)$$

$$= -(\mathbf{A}^X[\pi^X] - \mathbf{A}^Z[\pi^X])^\top \left(\sum_{i=1}^{|\pi^X|} \frac{\partial \mathbf{A}^Z[\pi^X]_i}{\partial \theta} \right), \quad (6)$$

where $|\pi^X|$ denotes the cardinality of a persistence pairing and $\mathbf{A}^Z[\pi^X]_i$ refers to the i^{th} entry of the vector of paired distances. This derivation works analogously for $\mathcal{L}_{Z \rightarrow X}$ (with π^X being replaced by π^Z). Furthermore, we note that any derivative of \mathbf{A}^X with respect to θ must vanish because the distances of the input samples do not depend on the encoding by definition.

3.4 Stability

While the general stability of persistence diagrams under small perturbations of the underlying space has already been established in Section 2, we still have to analyse the behaviour of our topological approximation on the level of mini-batches. The following theorem guarantees that subsampled persistence diagrams are close to the persistence diagrams of the point cloud X .

Theorem 1. *Let X be a point cloud of cardinality n and $X^{(m)}$ be one subsample of X of cardinality m , i.e. $X^{(m)} \subseteq X$, sampled without replacement. We can bound the probability of $X^{(m)}$ exceeding a threshold in terms of the bottleneck distance as*

$$\mathbb{P}(\text{d}_b(\mathcal{D}(X), \mathcal{D}(X^{(m)})) > \epsilon) \leq \mathbb{P}(\text{d}_H(X, X^{(m)}) > 2\epsilon), \quad (7)$$

where d_H refers to the Hausdorff distance between the point cloud and its subsample, i.e.

$$d_H(X, Y) := \max \left\{ \sup_{x \in X} \inf_{y \in Y} \text{dist}(x, y), \sup_{y \in Y} \inf_{x \in X} \text{dist}(x, y) \right\} \quad (8)$$

for a baseline distance $\text{dist}(x, y)$ such as the Euclidean distance.

Proof. See Section A.1 in the supplementary materials. \square

For $m \rightarrow n$, it is clear that $\lim_{m \rightarrow n} d_H(X, X^{(m)}) = 0$. Ideally, we want to bound the convergence rate of this expression. This is known to be feasible [13, 14], but requires more involved assumptions on the measures from which X and $X^{(m)}$ are sampled. Please refer to Section A.2 in the supplementary materials for an analysis of empirical convergence rates. Additionally, we can give a simple bound using the *diameter* $\text{diam}(X) := \sup\{\text{dist}(x, y) \mid x, y \in X\}$ by observing that $d_H(X, X^{(m)}) \leq \text{diam}(X)$ because the supremum is guaranteed to be an upper bound for the Hausdorff distance. This worst-case bound does not account for the sample size m . However, under certain independence assumptions, we can approximate the expected value of the Hausdorff distance $\mathbb{E}[d_H(X, X^{(m)})]$. The calculation of an exact representation is beyond the scope of this work and requires more tools from measure theory [49].

Theorem 2. Let $\mathbf{A} \in \mathbb{R}^{n \times m}$ be the distance matrix between samples of X and $X^{(m)}$, where the rows are sorted such that the first m rows correspond to the columns of the m subsampled points with diagonal elements $a_{ii} = 0$. Assume that the entries a_{ij} with $i > m$ are random samples following a distance distribution F_D with $\text{supp}(f_D) \in \mathbb{R}_{\geq 0}$. The minimal distances δ_i for rows with $i > m$ of \mathbf{A} follow a distribution F_Δ . Letting $Z := \max_{1 \leq i \leq n} \delta_i$ with a corresponding distribution F_Z , the expected Hausdorff distance between X and $X^{(m)}$ for $m < n$ is bounded by:

$$\mathbb{E}[d_H(X, X^{(m)})] = \mathbb{E}_{Z \sim F_Z}[Z] \leq \int_0^{+\infty} (1 - F_D(z)^{(n-1)}) dz \leq \int_0^{+\infty} (1 - F_D(z)^{m(n-m)}) dz \quad (9)$$

Proof. See Section A.3 in the supplementary materials. \square

Corollary 1. From Eq. 9, we obtain $\mathbb{E}[d_H(X, X^{(m)})] = 0$ as $m \rightarrow n$, so the expected value converges as the subsample size is sufficiently close to the total sample size.⁵

We conclude that our subsampling approach results in point clouds that are suitable proxies for the large-scale topological structures of the point cloud X .

4 Related work

Computational topology, in particular persistent homology (PH), has recently started gaining traction in several areas of machine learning research. We identify two major lines of research. First, PH is often used as a *post hoc* method for analysing topological characteristics of data sets. This leads to several publications that compare topological features of high-dimensional spaces with embeddings in order to assess the veracity or quality of a given embedding scheme [39, 44, 45, 54]. A recent publication Khrulkov and Oseledets [29] employs the same idea for comparing the sample spaces of GANs with their respective original data spaces, calculating the “geometry score” that measures to what extent topological features have been retained by a given model. More generally, PH can also be used to characterise the training of neural networks [25, 46] or their decision boundaries [42] in order to facilitate model selection. Our method crucially differs from all these publications in that we are able to obtain gradient information to *update* a model while training. The second line of research deals with integrating topological features in classifiers to increase classification performance. Hofer et al. [27] propose a new neural network layer that permits learning the best projection of persistence diagrams, which can subsequently be used as feature descriptors to classify graph-structured data. Likewise, different vectorisation strategies for persistence diagrams exist [1, 7], making it possible to

⁵For $m = n$, the two integrals switch order as $m(n - m) = 0 < n - 1$ (for $n > 1$).

use them in a variety of kernel-based classifiers. These strategies have recently been subsumed [8] in a novel architecture based on *deep sets* [55]. The commonality of all these approaches is that they treat persistence diagrams as a fixed quantity; while they are capable of learning suitable parameters for classifying them, they cannot adjust input data to better approximate a certain topology, for example.

These topology-based adjustments have only recently become feasible. Poulenard et al. [41] showed that under certain assumptions, it is possible to optimise real-valued functions based on their topology. This was the first approach to make it possible to align persistence diagrams by modifying input data itself; it is restricted to situations in which the connectivity of the data is known, i.e. a mesh exists, and the optimised functions have to be real-valued at the vertices of the mesh. By contrast, our method works directly on distances and sidesteps connectivity calculations by using the Vietoris–Rips complex. Chen et al. [16] use a similar optimisation technique to regularise the decision boundary of a classifier. This is perhaps the closest work to ours in spirit, but it is restricted to optimising the boundary of a classifier, whereas we want to align the input space and latent representations in a topologically meaningful manner. Moreover, our work does not require discretising the input space, which can be computationally expensive.

5 Experiments

We consider our main task to learn a latent space in an unsupervised manner such that topological features of the data space—measured using persistent homology approximation on every batch—are preserved as much as possible. We analyse latent representations in terms of (1) low-dimensional visualisations (to assess to what extent different structures or classes have been separated correctly), (2) reconstruction errors (to validate that our method does not adversely affect autoencoder performance), and (3) multi-scale density quality metrics (to measure the overall structure of the latent representation with respect to the original space).

5.1 Experimental Setup

Synthetic data set We use a SPHERES data set that consists of ten high-dimensional 100-spheres living in 101-dimensional space that are enclosed by an additional larger sphere that consists of the same amount of points as the total of inner spheres. For more details, please refer to Section A.4.

Real-world data sets We analyse two well-known image data sets, namely MNIST and FASHION-MNIST. These data sets are particularly amenable to our topology-based analysis because real-world images are known to lie *on or near* low-dimensional manifolds [5, 6, 23, 32, 40].

Baselines We compare our proposed approach against a set of deep and classic dimensionality reduction techniques. This includes UMAP [37], t-SNE [51], Isomap [50], PCA, as well as standard autoencoders. For the synthetic data set, we use an MLP autoencoder (3 layers per encoder and decoder); for MNIST and FASHION-MNIST, we use an architecture similar to DeepAE [26]. For further details, please refer to Section A.5.

Training We split each data set into training and testing (using the predefined split, if available, 90% versus 10% otherwise). Additionally, we remove 15% of the training split as validation data for tuning the hyperparameters. For details regarding the hyperparameter search, please refer to Section A.5. All autoencoders employ batch-norm and are optimized using ADAM [30]. Since t-SNE is not intended for applying to unseen test samples, we evaluate this method only on the train split. Due to significant computational scaling problems, we were not able to run a hyperparameter search on Isomap (which prevents a fair comparison for this algorithm) on the real-world data sets, so we can only compare against this algorithm on for the synthetic data sets.

5.2 Measuring the quality of latent representations

In order to assess the quality of our method, it is insufficient to merely consider the reconstruction error, as this quantity will merely tell us to what extent we can recover structures. Our primary interest concerns the quality of the latent space because, among others, it can be used to visualise the data set. While we initially considered classical quality metrics from non-linear dimensionality reduction (NLDR) algorithms [3, 24, 33–35, 45], we found that they are not suitable to determine to what extent local structures are being retained. In particular, we require a measure that is agnostic to

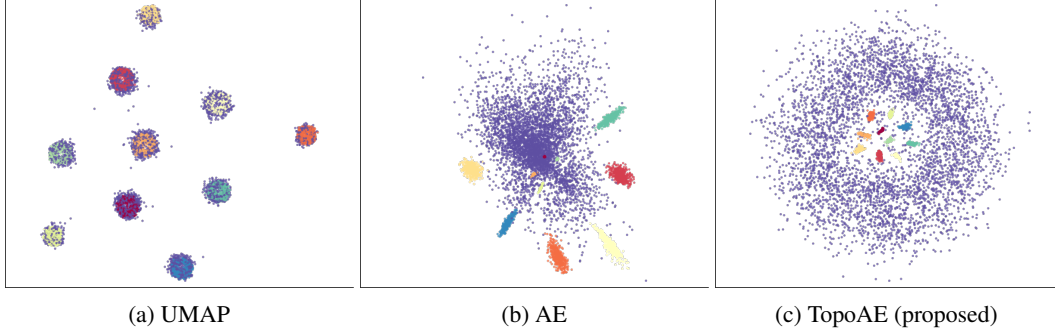


Figure 2: A selection of latent representations of the SPHERES data set. Only our method, here combined with the “vanilla” autoencoder architecture (AE), is capable of representing the complicated nesting relationship inherent to the data. See Figure A.2 in the supplementary materials for an extended version.

non-linear scaling of distances [52]. We thus propose a novel measure that is loosely based on the *distance to a measure density estimator* [10, 12].

Definition 1 (Density distribution error). *Let $\sigma \in \mathbb{R}_{>0}$. For a finite metric space \mathcal{S} with an associated distance $\text{dist}(\cdot, \cdot)$, we evaluate the density at each point $x \in \mathcal{S}$ as*

$$f_{\sigma}^{\mathcal{S}}(x) := \sum_{y \in \mathcal{S}} \exp\left(-\sigma^{-1} \text{dist}(x, y)^2\right), \quad (10)$$

where we assume without loss of generality that $\max \text{dist}(x, y) = 1$. We then calculate $f_{\sigma}^X(\cdot)$ and $f_{\sigma}^Z(\cdot)$, normalise them such that they sum to 1, and evaluate

$$\text{KL}_{\sigma} := \text{KL}\left(f_{\sigma}^X \parallel f_{\sigma}^Z\right), \quad (11)$$

i.e. the Kullback–Leibler divergence between the two density estimates.

We consider KL_{σ} to represent the error between the two density distributions. Ideally, we want the two distributions to be similar because this implies that density estimates in a low-dimensional representation are similar to the ones in the original space. In the subsequent comparisons, we will use KL_{σ} as well as (1) the *root mean square error* (RMSE), and (2) the *mean relative rank error* (MRRE), two classical measures from NLDR [33–35, 45].

5.3 Results

SPHERES Figure 2 depicts the latent representations of different methods. We observe that only our method—here, integrated into a “vanilla” autoencoder architecture (denoted with AE)—is capable of assessing the nesting relationship of the high-dimensional spheres correctly (Figure 2c). UMAP (Figure 2a), by contrast, “cuts open” the enclosing sphere, distributing most of its points evenly among the remaining spheres. We observe a similar behaviour for t-SNE (Figure A.2c in the appendix). In Table 1 we see that the density distribution error confirms the visual assessment that only our novel topological loss preserves the relevant structure of this dataset. The classical evaluation measures, however, favour UMAP, even though this method fails to capture the enclosing sphere manifold that accounts for half of the dataset.

FASHION-MNIST Figure 3 shows the latent representations of selected methods. We observe that, as we go from AE (“vanilla architecture”) to our proposed TopoAE, the relationship between different classes changes. For example, the red classes appear to be separate in the AE latent space, whereas they are merged in TopoAE and UMAP (which is also motivated in terms of preserving topological structures). We observe that, as opposed to AE, which is purely driven by the reconstruction error, our method has the additional objective of *preserving* structure, and not merely pulling different classes apart. The corresponding rows in Table 1 indicate that, over all scales, our methods ranks among the top two in terms of the density distribution error. On this data set, we observe that finding a *perfect* measure is non-trivial, as PCA is ranked favourably by all of them, while exhibiting a heterogeneous latent space (Figure A.3a in the supplementary materials).

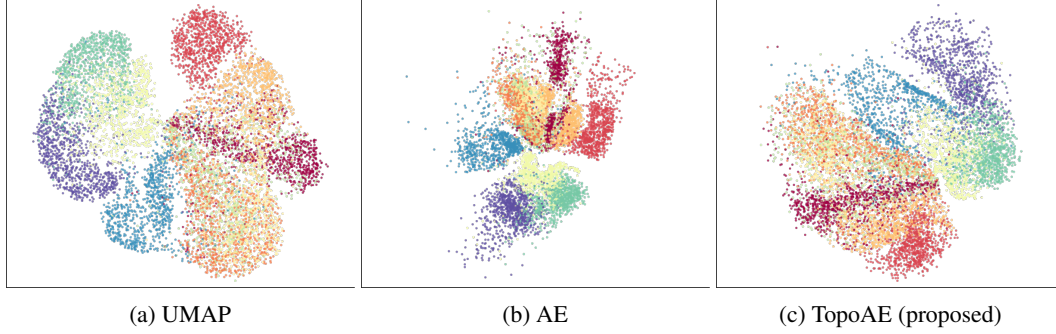


Figure 3: A selection of latent representations of the FASHION-MNIST data set. Please refer to Figure A.3 in the supplementary materials for an extended version.

Table 1: We display the following evaluation measures: the density distribution error KL_σ over multiple scales, the MRRE, and RMSE. Autoencoder reconstruction errors: (0.872, 0.119, 0.189) for TopoAE and (0.865, 0.100, 0.175) for AE.

Data set	Method	$KL_{0.01}$	$KL_{0.1}$	KL_1	MRRE	RMSE
SPHERES	UMAP	0.203729	0.553719	0.014364	0.243581	8.085793
	PCA	0.336197	0.648910	0.015219	0.293571	11.744817
	t-SNE	0.240239	0.397789	0.008836	0.248930	117.254678
	Isomap	0.181289	0.411020	0.008636	0.246400	10.987272
	AE	0.595361	0.662686	0.014052	0.325690	13.881863
	TopoAE (proposed)	0.080047	0.301653	0.006419	0.275201	11.965862
F-MNIST	UMAP	0.407057	0.062517	0.001544	0.029811	14.046468
	PCA	0.355832	0.052051	0.000688	0.057441	9.051018
	t-SNE	0.441658	0.058529	0.001654	0.035838	52.010151
	AE	0.428957	0.065549	0.001250	0.024195	21.251947
	TopoAE (proposed)	0.369017	0.044519	0.000734	0.032117	22.252948
MNIST	UMAP	0.321261	0.138753	0.002514	0.052364	14.493765
	PCA	0.389723	0.163971	0.001608	0.166031	13.175753
	t-SNE	0.268983	0.095210	0.001546	0.037108	18.558259
	AE	0.595782	0.099498	0.001325	0.084537	11.518178
	TopoAE (proposed)	0.246625	0.084069	0.000826	0.115594	18.191449

MNIST Here, Table 1 shows that our method TopoAE dominates the density distribution error, whereas t-SNE ranks thrice in the top two. While the corresponding embeddings (Figure A.4 in the appendix) demonstrate that UMAP and t-SNE are better at *clustering* the data set, they also lose some of the relationship information *between* clusters due to isolating individual digits.

6 Discussion and Conclusions

In this paper, we presented a topological autoencoder, a novel method for preserving topological information (measured in terms of persistent homology) of the input space when learning latent representations with deep neural networks. Under weak theoretical assumptions, we showed how our persistent homology (PH) calculations can be combined with backpropagation; moreover, we proved that approximating PH on the level of mini-batches is theoretically justified. In our experiments, we observed that our method is *uniquely* able to capture spatial relationships between nested high-dimensional spheres. This is relevant as the ability to cope with *several* manifolds in the domain of manifold learning still remains a challenging task. On real-world data sets, we observed that our topological loss leads to competitive performance in terms of preserving data space density, while not adversely affecting the reconstruction error.

In both synthetic and real-world data sets, we obtain interesting representations, as our method does not merely pull apart different classes, but tries to spatially arrange them meaningfully. Thus, we do not observe mere distinct “clouds”, but rather entangled structures, which we consider to constitute

a more meaningful representation of the underlying manifolds. Our topological loss calculation according to Section 3.3 is highly generic; it only requires the existence of a distance matrix between individual samples (either globally, or on the level of batches). As a consequence, our topological loss term can be directly integrated into a variety of different architectures and is *not* limited to standard autoencoders. For instance, we can also apply our constraint to variational setups (see Figure A.2 for a sketch).

Employing our generic constraint to more involved architectures will be an exciting route for future work. One issue with the calculation is that, given the computational complexity of calculating $\mathfrak{R}_\epsilon(\cdot)$, we scale progressively worse with increasing batch size. In future work, this could be mitigated by approximating the calculation of persistent homology [17, 28, 48] or by exploiting recent advances in parallelising it [2, 36].

Acknowledgements

We thank Christian Bock for fruitful discussions and valuable feedback.

References

- [1] H. Adams, T. Emerson, M. Kirby, R. Neville, C. Peterson, P. Shipman, S. Chepushtanova, E. Hanson, F. Motta, and L. Ziegelmeier. Persistence images: A stable vector representation of persistent homology. *Journal of Machine Learning Research*, 18(1):218–252, 2017.
- [2] U. Bauer, M. Kerber, and J. Reininghaus. Distributed computation of persistent homology. In C. C. McGeoch and U. Meyer, editors, *Proceedings of the Sixteenth Workshop on Algorithm Engineering and Experiments (ALENEX)*, pages 31–38. Society for Industrial and Applied Mathematics, 2014.
- [3] A. Bibal and B. Fréney. Measuring quality and interpretability of dimensionality reduction visualizations. *Safe Machine Learning workshop at ICLR*, 2019.
- [4] D. Burago, Y. Burago, and S. Ivanov. *A course in metric geometry*, volume 33 of *Graduate Studies in Mathematics*. American Mathematical Society, 2001.
- [5] G. Carlsson. Topology and data. *Bulletin of the American Mathematical Society*, 46(2):255–308, 2009.
- [6] G. Carlsson, T. Ishkhanov, V. De Silva, and A. Zomorodian. On the local behavior of spaces of natural images. *International Journal of Computer Vision*, 76(1):1–12, 2008.
- [7] M. Carrière, S. Y. Oudot, and M. Ovsjanikov. Stable topological signatures for points on 3D shapes. In *Proceedings of the Eurographics Symposium on Geometry Processing (SGP)*, pages 1–12, Aire-la-Ville, Switzerland, 2015. Eurographics Association.
- [8] M. Carrière, F. Chazal, Y. Ike, T. Lacombe, M. Royer, and Y. Umeda. A general neural network architecture for persistence diagrams and graph classification. *arXiv e-prints*, art. arXiv:1904.09378, 2019.
- [9] F. Chazal, D. Cohen-Steiner, L. J. Guibas, F. Mémoli, and S. Y. Oudot. Gromov–Hausdorff stable signatures for shapes using persistence. *Computer Graphics Forum*, 28(5):1393–1403, 2009.
- [10] F. Chazal, D. Cohen-Steiner, and Q. Mérigot. Geometric inference for probability measures. *Foundations of Computational Mathematics*, 11(6):733–751, 2011.
- [11] F. Chazal, V. de Silva, and S. Y. Oudot. Persistence stability for geometric complexes. *Geometriae Dedicata*, 173(1):193–214, 2014.
- [12] F. Chazal, B. T. Fasy, F. Lecci, B. Michel, A. Rinaldo, and L. Wasserman. Robust topological inference: Distance to a measure and kernel distance. *arXiv e-prints*, art. arXiv:1412.7197, 2014.

- [13] F. Chazal, B. Fasy, F. Lecci, B. Michel, A. Rinaldo, and L. Wasserman. Subsampling methods for persistent homology. In F. Bach and D. Blei, editors, *Proceedings of the 32nd International Conference on Machine Learning (ICML)*, volume 37 of *Proceedings of Machine Learning Research*, pages 2143–2151. PMLR, 2015.
- [14] F. Chazal, M. Glisse, C. Labruère, and B. Michel. Convergence rates for persistence diagram estimation in topological data analysis. *Journal of Machine Learning Research*, 16:3603–3635, 2015.
- [15] F. Chazal, V. de Silva, M. Glisse, and S. Oudot. *The structure and stability of persistence modules*. SpringerBriefs in Mathematics. Springer, Heidelberg, Germany, 2016.
- [16] C. Chen, X. Ni, Q. Bai, and Y. Wang. A topological regularizer for classifiers via persistent homology. In K. Chaudhuri and M. Sugiyama, editors, *Proceedings of Machine Learning Research*, volume 89 of *Proceedings of Machine Learning Research*, pages 2573–2582. PMLR, 2019.
- [17] A. Choudhary, M. Kerber, and S. Raghvendra. Improved topological approximations by digitization. *arXiv e-prints*, art. arXiv:1812.04966, 2018.
- [18] D. Cohen-Steiner, H. Edelsbrunner, and J. Harer. Stability of persistence diagrams. *Discrete & Computational Geometry*, 37(1):103–120, 2007.
- [19] T. H. Cormen, C. E. Leiserson, R. L. Rivest, and C. Stein. *Introduction to algorithms*. MIT Press, Cambridge, MA, USA, 3 edition, 2009.
- [20] H. Edelsbrunner and J. Harer. Persistent homology—a survey. In J. E. Goodman, J. Pach, and R. Pollack, editors, *Surveys on discrete and computational geometry: Twenty years later*, number 453 in Contemporary Mathematics, pages 257–282. American Mathematical Society, Providence, RI, USA, 2008.
- [21] H. Edelsbrunner and D. Morozov. Persistent homology: Theory and practice. In R. Latała, A. Ruciński, P. Strzelecki, J. Świątkowski, D. Wrzosek, and P. Zakrzewski, editors, *European Congress of Mathematics*. European Mathematical Society Publishing House, Zürich, Switzerland, 2014.
- [22] H. Edelsbrunner, D. Letscher, and A. J. Zomorodian. Topological persistence and simplification. *Discrete & Computational Geometry*, 28(4):511–533, 2002.
- [23] C. Fefferman, S. Mitter, and H. Narayanan. Testing the manifold hypothesis. *Journal of the American Mathematical Society*, 29(4):983–1049, 2016.
- [24] A. Gracia, S. González, V. Robles, and E. Menasalvas. A methodology to compare dimensionality reduction algorithms in terms of loss of quality. *Information Sciences*, 270:1–27, 2014.
- [25] W. H. Guss and R. Salakhutdinov. On characterizing the capacity of neural networks using algebraic topology. *arXiv e-prints*, art. arXiv:1802.04443, 2018.
- [26] G. E. Hinton and R. R. Salakhutdinov. Reducing the dimensionality of data with neural networks. *science*, 313(5786):504–507, 2006.
- [27] C. Hofer, R. Kwitt, M. Niethammer, and A. Uhl. Deep learning with topological signatures. In I. Guyon, U. V. Luxburg, S. Bengio, H. Wallach, R. Fergus, S. Vishwanathan, and R. Garnett, editors, *Advances in Neural Information Processing Systems 30*, pages 1633–1643. Curran Associates, Inc., 2017.
- [28] M. Kerber and R. Sharathkumar. Approximate čech complexes in low and high dimensions. *arXiv e-prints*, art. arXiv:1307.3272, 2013.
- [29] V. Khrulkov and I. Oseledets. Geometry score: A method for comparing generative adversarial networks. In J. Dy and A. Krause, editors, *Proceedings of the 35th International Conference on Machine Learning*, volume 80 of *Proceedings of Machine Learning Research*, pages 2621–2629. PMLR, 2018.

- [30] D. P. Kingma and J. Ba. Adam: A method for stochastic optimization. *arXiv preprint arXiv:1412.6980*, 2014.
- [31] V. Kurlin. A one-dimensional homologically persistent skeleton of an unstructured point cloud in any metric space. *Computer Graphics Forum*, 34(5):253–262, 2015.
- [32] A. B. Lee, K. S. Pedersen, and D. Mumford. The nonlinear statistics of high-contrast patches in natural images. *International Journal of Computer Vision*, 54(1–3):83–103, 2003.
- [33] J. A. Lee and M. Verleysen. Quality assessment of nonlinear dimensionality reduction based on k -ary neighborhoods. In Y. Saeys, H. Liu, I. Inza, L. Wehenkel, and Y. Van de Pee, editors, *Proceedings of the Workshop on New Challenges for Feature Selection in Data Mining and Knowledge Discovery at ECML/PKDD 2008*, volume 4 of *Proceedings of Machine Learning Research*, pages 21–35. PMLR, 2008.
- [34] J. A. Lee and M. Verleysen. Quality assessment of dimensionality reduction: Rank-based criteria. *Neurocomputing*, 72(7):1431–1443, 2009. ISSN 0925-2312.
- [35] J. A. Lee, D. H. Peluffo-Ordóñez, and M. Verleysen. Multi-scale similarities in stochastic neighbour embedding: Reducing dimensionality while preserving both local and global structure. *Neurocomputing*, 169:246–261, 2015.
- [36] R. Lewis and D. Morozov. Parallel computation of persistent homology using the blowup complex. In *Proceedings of the 27th ACM Symposium on Parallelism in Algorithms and Architectures (SPAA)*, pages 323–331. ACM, 2015.
- [37] L. McInnes, J. Healy, and J. Melville. Umap: Uniform manifold approximation and projection for dimension reduction. *arXiv preprint arXiv:1802.03426*, 2018.
- [38] F. Méoli and G. Sapiro. Comparing point clouds. In *Proceedings of the 2004 Eurographics/ACM SIGGRAPH Symposium on Geometry Processing (SGP)*, pages 32–40, New York, NY, USA, 2004. ACM.
- [39] R. Paul and S. K. Chalup. A study on validating non-linear dimensionality reduction using persistent homology. *Pattern Recognition Letters*, 100:160–166, 2017.
- [40] G. Peyré. Manifold models for signals and images. *Computer Vision and Image Understanding*, 113(2):249–260, 2009.
- [41] A. Poulenard, P. Skraba, and M. Ovsjanikov. Topological function optimization for continuous shape matching. *Computer Graphics Forum*, 37(5):13–25, 2018.
- [42] K. N. Ramamurthy, K. R. Varshney, and K. Mody. Topological data analysis of decision boundaries with application to model selection. *arXiv e-prints*, art. arXiv:1805.09949, 2018.
- [43] J. Reininghaus, S. Huber, U. Bauer, and R. Kwitt. A stable multi-scale kernel for topological machine learning. In *Proceedings of the IEEE Conference on Computer Vision and Pattern Recognition*, pages 4741–4748, 2015.
- [44] B. Rieck and H. Leitte. Persistent homology for the evaluation of dimensionality reduction schemes. *Computer Graphics Forum*, 34(3):431–440, 2015.
- [45] B. Rieck and H. Leitte. Agreement analysis of quality measures for dimensionality reduction. In H. Carr, C. Garth, and T. Weinkauff, editors, *Topological Methods in Data Analysis and Visualization IV*. Springer International Publishing, Cham, Switzerland, 2017.
- [46] B. Rieck, M. Togninalli, C. Bock, M. Moor, M. Horn, T. Gumbsch, and K. Borgwardt. Neural persistence: A complexity measure for deep neural networks using algebraic topology. In *International Conference on Learning Representations (ICLR)*, 2019.
- [47] T. scikit-optimize contributors. scikit-optimize/scikit-optimize: v0.5.2, Mar. 2018. <https://doi.org/10.5281/zenodo.1207017>.
- [48] D. R. Sheehy. Linear-size approximations to the Vietoris–Rips filtration. *Discrete & Computational Geometry*, 49(4):778–796, 2013.

- [49] A. Singh, C. Scott, and R. Nowak. Adaptive Hausdorff estimation of density level sets. *The Annals of Statistics*, 37(5B):2760–2782, 2009.
- [50] J. B. Tenenbaum, V. De Silva, and J. C. Langford. A global geometric framework for nonlinear dimensionality reduction. *Science*, 290(5500):2319–2323, 2000.
- [51] L. J. van der Maaten and G. Hinton. Visualizing data using t-SNE. *Journal of Machine Learning Research*, 9:2579–2605, 2008.
- [52] L. J. van der Maaten, E. O. Postma, and H. J. van den Herik. Dimensionality reduction: A comparative review. Technical Report 2009-005, Tilburg University, 2009.
- [53] L. Vietoris. Über den höheren Zusammenhang kompakter Räume und eine Klasse von zusammenhangstreuen Abbildungen. *Mathematische Annalen*, 97(1):454–472, 1927.
- [54] L. Yan, Y. Zhao, P. Rosen, C. Scheidegger, and B. Wang. Homology-preserving dimensionality reduction via manifold landmarking and tearing. *arXiv e-prints*, art. arXiv:1806.08460, 2018.
- [55] M. Zaheer, S. Kottur, S. Ravanbakhsh, B. Poczos, R. R. Salakhutdinov, and A. J. Smola. Deep sets. In I. Guyon, U. V. Luxburg, S. Bengio, H. Wallach, R. Fergus, S. Vishwanathan, and R. Garnett, editors, *Advances in Neural Information Processing Systems 30*, pages 3391–3401. Curran Associates, Inc., 2017.
- [56] A. J. Zomorodian. Fast construction of the Vietoris–Rips complex. *Computers & Graphics*, 34(3):263–271, 2010.

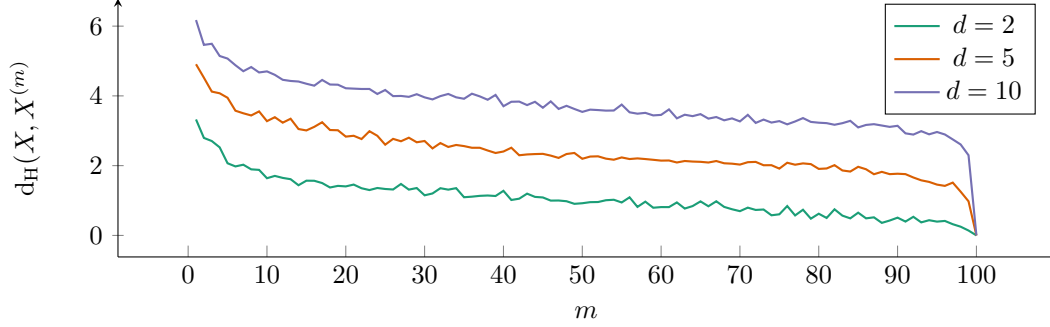


Figure A.1: Empirical convergence rate (mean) of the Hausdorff distance for a subsample of size m of 100 points in a d -dimensional space, following a standard normal distribution.

A Appendix

A.1 Proof of Theorem 1

Proof. The stability of persistent homology calculations was proved by Chazal et al. [11] for finite metric spaces. More precisely, given two metric spaces X and Y , we have

$$d_b(\mathcal{D}(X), \mathcal{D}(Y)) \leq 2 d_{GH}(X, Y), \quad (12)$$

where $d_{GH}(X, Y)$ refers to the Gromov–Hausdorff distance [4, p. 254] of the two spaces. It is defined as the infimum Hausdorff distance over all isometric embeddings of X and Y . This distance can be employed for shape comparison [9, 38], but is hard to compute. In our case, with $X = X$ and $Y = X^{(m)}$, we consider both spaces to have the same metric (for Y , we take the canonical restriction of the metric from X to the subspace Y). By definition of the Gromov–Hausdorff distance, we thus have $d_{GH}(X, Y) \leq d_H(X, Y)$, so Eq. 8 leads to

$$d_b(\mathcal{D}(X), \mathcal{D}(Y)) \leq 2 d_H(X, Y), \quad (13)$$

from which the original claim from Eq. 7 follows by taking probabilities on both sides. \square

A.2 Empirical convergence rates of $d_H(X, X^{(m)})$

Figure A.1 depicts the mean of the convergence rate (mean) of the Hausdorff distance for a subsample of size m of 100 points in a d -dimensional space, following a standard normal distribution. We can see that the convergence rate is roughly similar, but shown on different absolute levels that depend on the ambient dimension.

A.3 Proof of Theorem 2

Prior to the proof we state two observations that arise from our special setting of dealing with finite point clouds.

Observation 1. Since $X^{(m)} \subseteq X$, we have $\sup_{x' \in X^{(m)}} \inf_{x \in X} \text{dist}(x, x') = 0$. Hence, the Hausdorff distance simplifies to:

$$d_H(X, X^{(m)}) := \sup_{x \in X} \inf_{x' \in X^{(m)}} \text{dist}(x, x') \quad (14)$$

In other words, we only have to consider a “one-sided” expression of the distance because the distance from the subsample to the original point cloud is always zero.

Observation 2. Since our point clouds of interest are finite sets, the suprema and infima of the Hausdorff distance coincide with the maxima and minima, which we will subsequently use for easier readability.

Hence, the computation of $d_H(X, X^{(m)})$ can be divided into three steps.

1. Using the baseline distance $\text{dist}(\cdot, \cdot)$, we compute a distance matrix $\mathbf{A} \in \mathbb{R}^{n \times m}$ between all points in X and $X^{(m)}$.
2. For each of the n points in X , we compute the minimal distance to the m samples of $X^{(m)}$ by extracting the minimal distance per row of \mathbf{A} and gather all minimal distances in $\delta \in \mathbb{R}^n$.
3. Finally, we return the maximal entry of δ as $d_H(X, X^{(m)})$.

In the subsequent proof, we require an independence assumption of the samples.

Proof. Using Observations 1 and 2 we obtain a simplified expression for the Hausdorff distance, i.e.

$$d_H(X, X^{(m)}) := \max_{i, 1 \leq i \leq n} \left(\min_{j, 1 \leq j \leq m} (a_{ij}) \right). \quad (15)$$

The minimal distances of the first m rows of \mathbf{A} are trivially 0. Hence, the outer maximum is determined by the remaining $n - m$ row minima $\{\delta_i \mid m < i \leq n\}$ with $\delta_i = \min_{1 \leq j \leq m} (a_{ij})$. Those minima follow the distribution $F_\Delta(y)$ with

$$F_\Delta(y) = \mathbb{P}(\delta_i \leq y) = 1 - \mathbb{P}(\delta_i > y) = 1 - \mathbb{P}\left(\min_{1 \leq j \leq m} a_{ij} > y\right) \quad (16)$$

$$= 1 - \mathbb{P}\left(\bigcap_j a_{ij} > y\right) = 1 - (1 - F_D(y))^m = F_D(y)^m. \quad (17)$$

Next, we consider $Z := \max_{1 \leq i \leq n} \delta_i$. To evaluate the density of Z , we first need to derive its distribution F_Z :

$$F_Z(z) = \mathbb{P}(Z \leq z) = \mathbb{P}\left(\max_{m < i \leq n} \delta_i \leq z\right) = \mathbb{P}\left(\bigcap_{m < i \leq n} \delta_i \leq z\right) \quad (18)$$

Next, we approximate Z by Z' by imposing *i.i.d sampling* of the minimal distances δ_i from F_Δ . This is an approximation because in practice, the rows $m + 1$ to n are not stochastically independent because of the triangular inequality that holds for metrics. However, assuming i.i.d., we arrive at

$$F_{Z'}(z) = F_\Delta(z)^{n-m} \quad (19)$$

. Since Z' has positive support its expectation can then be evaluated as:

$$\mathbb{E}_{Z' \sim F_{Z'}}[Z'] = \int_0^{+\infty} (1 - F_{Z'}(z)) dz = \int_0^{+\infty} (1 - F_\Delta(z)^{n-m}) dz \quad (20)$$

$$= \int_0^{+\infty} (1 - F_D(z)^{m(n-m)}) dz \geq \int_0^{+\infty} (1 - F_D(z)^{(n-1)}) dz \quad (21)$$

The independence assumption leading to Z' results in *overestimating* the variance of the drawn minima δ_i . Thus, the expected maximum of those minima, $\mathbb{E}[Z']$, is overestimating the actual expectation of the maximum $\mathbb{E}[Z]$, which is why Eq. 20 to Eq. 21 constitute an *upper bound* of $\mathbb{E}[Z]$, and equivalently, an upper bound of $\mathbb{E}[d_H(X, X^{(m)})]$. When increasing m , $\mathbb{E}[d_H(X, X^{(m)})]$ decreases monotonically since for a particular m , we draw $n - m$ samples from the minimal distance distribution F_Δ , and their maximum determines the Hausdorff distance. In contrast, our preliminary upper bound on the left-hand side of Eq. 21 forms a downwards-facing parabola due to the quadratic form in the exponent. This indicates that a tighter bound is achieved for $m \neq n$ by using the minimal subsample size of $m = 1$.

□

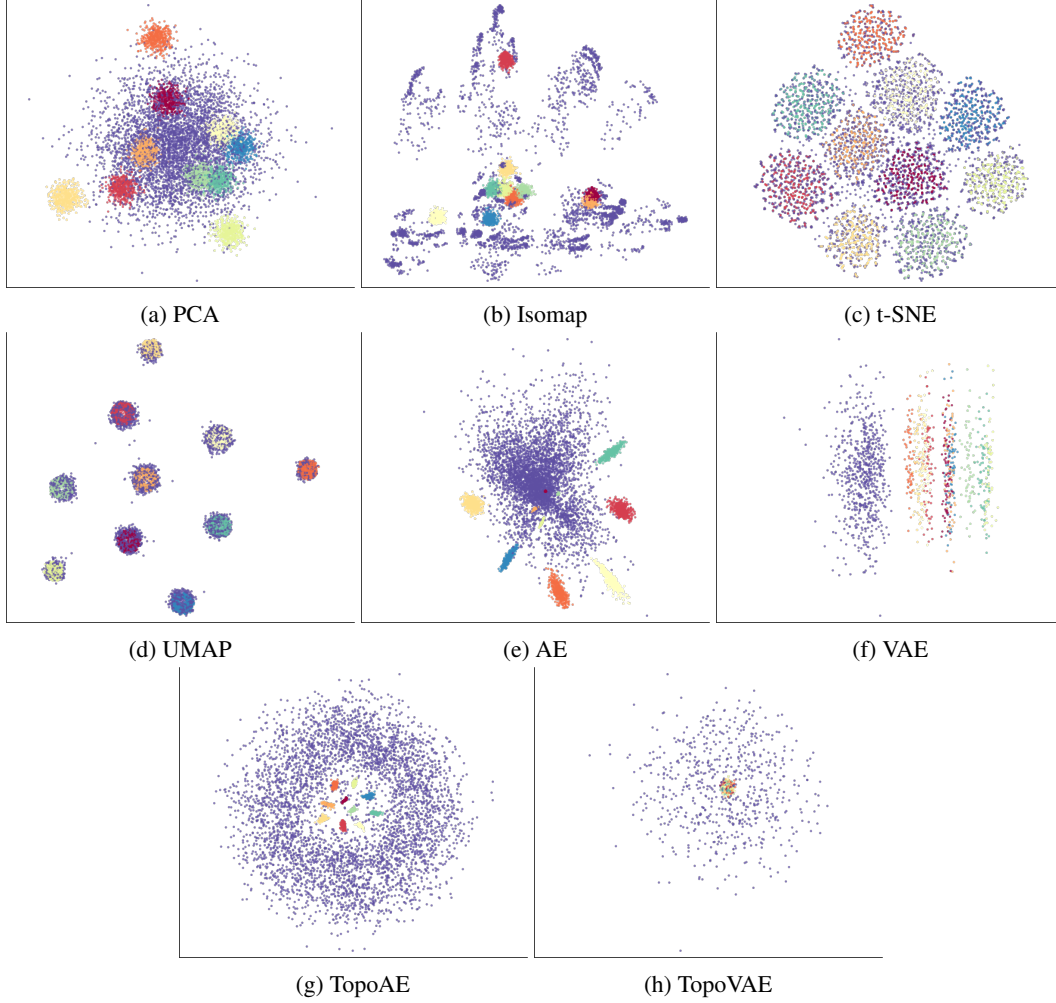


Figure A.2: A depiction of *all* latent spaces obtained for the SPHERES data set. This is an extension of the figure shown in Section 5.3. It permits a comparison with a larger set of methods.

A.4 Synthetic Dataset

SPHERES consists of eleven high-dimensional 100-spheres living in 101-dimensional space. Ten spheres of radius $r = 5$ are each shifted in a random direction (by adding the same Gaussian noise vector per sphere). To this end, we draw ten d -dimensional Gaussian vectors following $\mathcal{N}(\mathbf{0}, \mathbf{I}^{(10/\sqrt{d})})$ for $d = 101$. Crucially, to add interesting topological information to the data set, the ten spheres are enclosed by an additional larger sphere of radius $5r$. The spheres were generated using the library `scikit-tda`.

A.5 Architectures and Hyperparameter Tuning

Architectures for synthetic datasets For the synthetically generated datasets we use a simple Multilayer perceptron architecture consisting of two hidden layer with 32 neurons each both encoder and decoder and a bottleneck of two neurons such that the sequence of hidden-layer neurons is $32 - 32 - 2 - 32 - 32$. ReLU non-linearities and batch normalization were applied between the layers excluding the output layer and the bottleneck layer. The networks were fit using mean squared error loss.

Architectures for MNIST and Fashion MNIST For the MNIST and FASHION-MNIST datasets, we use an architecture inspired by DeepAE [26]. This architecture is composed of 3 layers of hidden

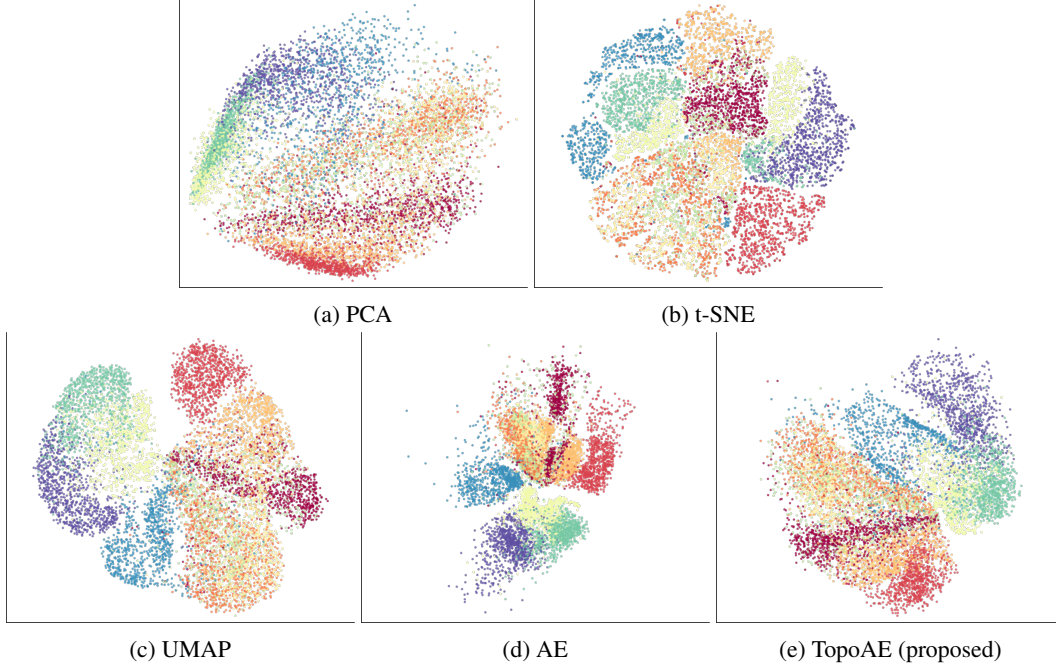


Figure A.3: A selection of latent representations of the FASHION-MNIST data set. This is an extension of the figure shown in Section 5.3, permitting a comparison with a larger set of methods.

neurons of decreasing size ($1000 - 500 - 250$) for the encoder part, a bottleneck of two neurons, and a sequence of three layers of hidden neurons in decreasing size ($250 - 500 - 1000$) for the decoder. In contrast to the originally proposed architecture, we applied ReLU non-linearities and batch normalization between the layers as we observed faster and more stable training. For the non-linearities of the final layer, we applied the *tanh* non-linearity, such that the image of the activation matches the range of input images scaled between -1 and 1 . Also here we applied mean squared error loss.

All neural network architectures were fit using Adam and weight-decay of 10^{-5} .

Hyperparameter tuning For hyperparameter tuning we apply a Bayesian optimization framework provided by the *scikit-optimize* library [47] with 40 calls per method on the synthetic datasets and 20 calls per method on the MNIST and FASHIONMNIST datasets. We select the best model parameters in terms of density distribution error on the validation split and evaluate and report it on the test split.

Neural networks For the neural networks we sample the learning rate log-uniformly in the range $10^{-4} - 10^{-2}$, and for the TopoAE method we sample the regularization strength log-uniformly in the range $10^{-2} - 1$.

Competitor methods For T-SNE we sample the perplexity uniformly in the range $5 - 50$ and the learning rate log-uniformly in the range $10 - 1000$. For Isomap and UMAP, the number of neighbors included in the computation was varied between $15 - 500$. For UMAP, we additionally vary the *min_dist* parameter uniformly between 0 and 1 .

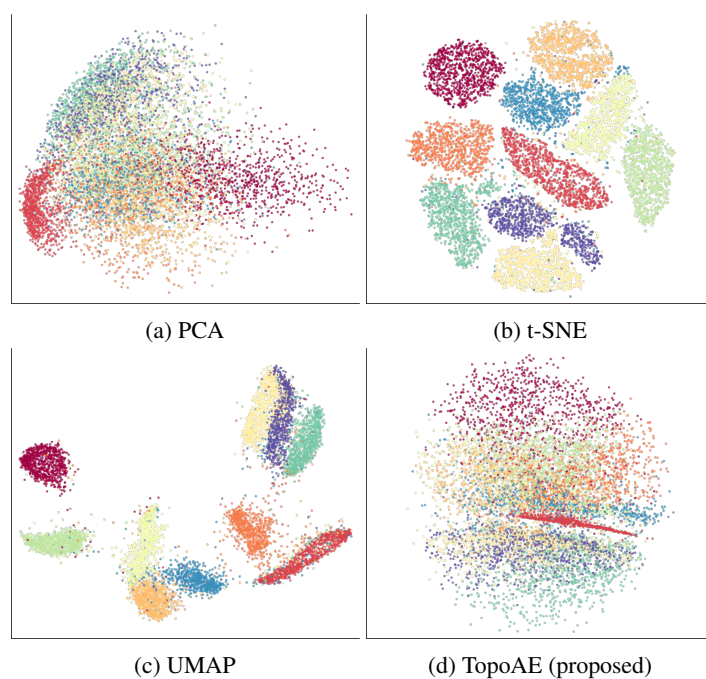


Figure A.4: A selection of latent representations of the MNIST data set. This is an extension of the figure shown in Section 5.3, permitting a comparison with a larger set of methods.